HHS Public Access

Author manuscript

J Occup Environ Hyg. Author manuscript; available in PMC 2020 August 01.

Published in final edited form as:

J Occup Environ Hyg. 2019 August ; 16(8): 564–574. doi:10.1080/15459624.2019.1628965.

Sources of error and variability in particulate matter sensor network measurements

Christopher Zuidema[a], **Larissa V. Stebounova**[b], **Sinan Sousan**[b,c], **Geb Thomas**[d], **Kirsten Koehler**[e], **Thomas M. Peters**[b]

[a]Department of Environmental and Occupational Health Sciences, University of Washington, Seattle, Washington [b]Department of Occupational and Environmental Health, University of Iowa, Iowa City, Iowa [c]Department of Public Health, East Carolina University/North Carolina Agromedicine Institute, Greenville, North Carolina [d]Department of Industrial and Systems Engineering, University of Iowa, Iowa City, Iowa [e]Department of Environmental Health and Engineering, Johns Hopkins Bloomberg School of Public Health, Baltimore, Maryland

Abstract

The quality of mass concentration estimates from increasingly popular networks of low-cost particulate matter sensors depends on accurate conversion of sensor output (e.g., voltage) into gravimetric-equivalent mass concentration, typically using a calibration procedure. This study evaluates two important sources of variability that lead to error in estimating gravimetric-equivalent mass concentration: the temporal changes in sensor calibration and the spatial and temporal variability in gravimetric correction factors. A 40-node sensor network was deployed in a heavy vehicle manufacturing facility for 8 months. At a central location in the facility, particulate matter was continuously measured with three sensors of the network and a traditional, higher-cost photometer, determining the calibration slope and intercept needed to translate sensor output to photometric-equivalent mass concentration. Throughout the facility, during three intensive sampling campaigns, respirable mass concentrations were measured with gravimetric samplers and photometers to determine correction factors needed to adjust photometric-equivalent to gravimetric-equivalent mass concentration. Both field-determined sensor calibration slopes and intercepts were statistically different than those estimated in the laboratory ($\alpha = 0.05$), emphasizing the importance of aerosol properties when converting voltage to photometric-equivalent mass concentration and the need for field calibration to determine slope. Evidence suggested the sensors' weekly field calibration slope decreased and intercept increased, indicating the sensors were deteriorating over time. The mean correction factor in the cutting and shot blasting area (2.9) was substantially and statistically lower than that in the machining and welding area (4.6; $p = 0.01$). Therefore, different correction factors should be determined near different occupational processes to accurately estimate particle mass concentrations.

CONTACT Thomas M. Peters thomas-m-peters@uiowa.edu Department of Occupational and Environmental Health, 105 River St, S331 CPHB, University of Iowa, Iowa City, IA 52242-5000.

Supplemental data for this article is available online at at tandfonline.com/uoeh. AIHA and ACGIH members may also access supplementary material at http://uoeh.tandfonline.com/.

Keywords

Correction factor; field calibration; low-cost sensors; particle composition; particulate matter concentration; photometer

Introduction

Occupational exposure to particulate matter (PM) is responsible for increased morbidity and mortality from cardiovascular and respiratory diseases and elevated risk of lung cancer in workers.[1-4] In the United States, the Occupational Safety and Health Administration (OSHA) regulates that a workplace maintains exposures below permissible exposure limits (PELs). For respirable particles not otherwise regulated, the PEL is 5 mg/m^3 expressed as an 8-hr, time-weighted average (TWA).[5] The American Conference of Governmental Industrial Hygienists (ACGIH®) recommends an 8-hr, threshold limit value-TWA of 3 mg/m^3 for respirable particles not otherwise specified.[6] These limits are almost 1,000 times higher than those applicable to ambient air, such as the 24-hr National Ambient Air Quality Standard for particulate matter smaller than 2.5 μm of 35 $\mu g/m^3$.

Worker exposure is typically measured with gravimetric personal samplers. Gravimetric personal samplers physically collect particles from within the breathing zone onto a filter, which is weighed before- and-after sampling. The TWA mass concentration, calculated from the weight gain of the filter divided by the volume of air sampled, is then compared with the appropriate occupational exposure limit. Although a direct measure of mass concentration, gravimetric personal sampling requires substantial manual effort, cost, and lacks the temporal resolution to correlate peak exposures with particular working activities.

In contrast, commercial photometers (~$3,000–$10,000), such as personal DataRAMs (pDRs) from ThermoFisher Scientific (Waltham, MA), can be used for continuous monitoring of personal PM exposures in occupational settings.[7,8] They provide a near-real-time indication of mass concentration inferred from the light scattered by an assembly of particles over a small angle, typically at 90 degrees from the incident light.[9] The measured photometric-equivalent mass concentration is highly dependent on particle composition, refractive index, size, and morphology, and a correction factor (CF) (sometimes called “calibration factor” in the literature) is often used to adjust the photometric-equivalent mass concentration to gravimetric-equivalent mass concentration.[10-12] The CF is calculated as the mass concentration measured with a personal filter sampler divided by that measured with a co-located photometer over the same time period.[13] In a review of previously published studies, Fischer and Koshland[14] reported CFs between pDR1000 and gravimetric samples ranged from 0.6 to 2.3. The same authors found CFs in rural Chinese kitchens, where 24-hr aerosol concentrations were as high as 700 $\mu g/m^3$, ranged from 0.78 to 7.4, and for samples with relative humidity <95% (n = 16), a geometric mean ± geometric standard deviation of 2.13 ± 1.47.[14] Direct-reading instruments, like pDRs, can be used in roving monitoring, which requires the instrument be physically moved from location to location, to create maps of concentration across the workplace.[15-20] They could be used in a network of

stationary monitors to capture a time-series of such maps, although their high cost prohibits use in this way.[19]

Recently, small, low-cost sensors for PM have proliferated in the marketplace,[21] making possible a sensor network to capture maps of particle concentration with high spatial and temporal resolution. Many of these sensors are photometers, using optical components and geometry similar to more expensive photometers, such as pDRs. The sensor output (e.g., voltage) must be converted to PM mass concentration after a calibration procedure, commonly done using higher-cost photometers.[22] Such sensors have been extensively used to monitor particle concentrations in occupational and environmental settings.[21,23,24] Their small size and low cost makes them attractive for use in a network to map aerosol concentrations in a workplace in real-time.[25] However, challenges in using these sensors within a network include lower accuracy and precision compared to traditional photometers such as pDRs, reduced stability over time due to sensor fouling, and a necessity for thorough laboratory and field calibration.[25,26]

An 8-month deployment of a multi-hazard sensor network in a heavy vehicle manufacturing facility was previously described that included the measurement of respirable mass concentration with 40 low-cost sensor nodes positioned at 38 unique locations.[25] In our previous work, several sources of uncertainty were estimated when using low-cost sensors. The first is the variability among individual units, for which a method was developed to compare individual units and identify those that behave most similarly for field deployment.[22] For deployment, 100 sensors were evaluated in the laboratory to identify 50 that had the most similar slope of response to PM mass concentration.

After deployment, two additional sources of variability that can lead to errors in measurement of PM with low-cost sensors persist: (1) the time dependence of the calibration parameters (sensor slope and intercept) caused by sensor drift, changes in electronics, and fouling of the sensor; and (2) the aerosol composition dependence of the slope (accounting for changes in size distribution, chemical composition and refractive index). In the previous study, the time dependence of the calibration intercept was identified as a major source of uncertainty in the mass concentrations measured by PM sensors. A practical solution was developed to address this for all the sensors in the network. Low aerosol mass concentration periods during nonproduction times (i.e., Sunday night) was used to estimate weekly intercepts for each sensor.[25] Both the temporal variability of calibration parameters and the temporal and spatial variability of CFs will lead to errors in measurement of aerosol concentration if not accounted for. In the present study, the temporal variability in sensor calibration slope and intercept was further analyzed by focusing on three co-located sensors deployed in the field alongside a traditional photometer during an 8-month period of time. The role of aerosol composition on the accuracy of mass-based measures of aerosol concentration in a workplace was also considered.

Methods

Study site and sensor network

A multi-hazard sensor network was operated for 8 months (August 2017 to March 2018) within 74,900 m^2 (806,400 ft^2) of a +185,800 m^2 (+2-million ft^2) manufacturing facility that produces heavy vehicles for construction and forestry. In this facility, various metalworking processes contribute to different aerosol concentrations and compositions. First, pieces are cut from large metal sheets with torches and lasers. The surfaces of these pieces are prepared by abrasive blasting before being manually tacked together and readied for robotic welding into vehicle components. Workers finish welds that cannot be completed robotically and grind excess materials from components. Features are then added to components by automated machining.

The manufacturing floor is one contiguous space containing collections of equipment and manufacturing activities as indicated on the floorplan of the facility (Figure 1). The manufacturing floor was grouped into three areas based on general manufacturing processes and location. Because manufacturing areas are not physically isolated from one another, there is the potential for aerosols generated in one area to be transported to other areas. For example, metal fume from welding could be transported throughout the rest of the manufacturing floor. General ventilation serves the whole manufacturing floor, in addition, torch and laser cutting and abrasive blasting equipment is enclosed and are the only processes served by local exhaust ventilation. At 38 unique locations within the facility, a monitor with sensors for PM, carbon monoxide, oxidizing gases, and noise was attached on a vertical I-beam approximately 3 m from the floor.[24] An additional two monitors were deployed at one of those locations subsequently referred to as the “central” location. Measurements from each monitor were transmitted wirelessly to a database approximately every 5 min.

Laboratory calibration and sensor selection

Low-cost sensors for PM (GP2Y1010AU0F, Sharp Electronics, Osaka, Japan) were selected through a laboratory calibration procedure using salt aerosol. As described in detail previously,[22] 50 PM sensors were selected from 100 with calibration slopes that were most similar (slopes within ±14% of mean). Of those 50 sensors, the three with the median, maximum, and minimum slopes (sensor 1: 1054 mV/(mg/m^3), sensor 2: 1189 mV/(mg/m^3), and sensor 3: 971 mV/(mg/m^3), respectively) were installed in monitors positioned at the central location. As part of this selection procedure based on sensor slope, the calibration intercept was also determined for each sensor (sensor 1: 693 mV, sensor 2: 616 mV, and sensor 3: 984 mV). Monitors with sensors randomly selected from those remaining were placed at the other 37 locations throughout the facility. Ten monitors were retained for backup.

Field calibration parameters

A personal DataRam 1000 photometer (pDR1000, ThermoFisher Scientific, Waltham, MA) and three co-located sensors were placed at the central location. The pDR1000, calibrated immediately before this study, was selected because it samples the air passively, which

enables the unit to run for long times in contaminated environments. The pDR1000 has been described previously by other researchers.[7,27] Due to data storage limitations, the pDR1000 was set to log every 10 min throughout the study, except when the team was on-site, when logging was set to 5 min. The reading from the pDR1000 when immersed in clean, filtered air was measured as 0 ± 0.020 mg/m^3 at the beginning, middle, and end of the study. Ordinary least squares linear regression was performed over the entire study period and weekly to translate the PM sensor response (mV) from each low-cost PM sensor at the central location (n = 3) to the photometric-equivalent mass concentration measured by the pDR1000.

Gravimetric correction factors

CFs were determined to adjust photometric-equivalent to gravimetric-equivalent respirable mass concentration for the day shift (6–8 hr per day) for 1 d in August, 2 d in December, and 2 d in March throughout the facility at the locations identified in Figure 1. At the central location, respirable samplers (37-mm aluminum cyclones, SKC Inc., Eighty Four, PA; Teflo, polytetrafluoroethylene, PTFE, membrane filter, R2PJ037, PALL, Ann Arbor, MI; sampling pump, GilAir Plus, Sensidyne, St. Petersburg, FL) were operated at an airflow rate of 2.5 L/min. At other locations, photometers equipped with integrated sample filters (pDR1500, ThermoFisher Scientific, Waltham, MA) were used to measure both direct-reading photometric-equivalent mass concentration and time-integrated gravimetric mass concentration. Personal measurements were also taken by a member of the study staff wearing a pDR1500 for 6–8 hr per day while traveling throughout the facility, providing an estimate of a facility-wide average CF. Glass microfiber filters (37 mm, P/N 1827-037, Whatman, Maidstone, UK) were used in the pDR1500s. The pDR1500s were set to log every five mins and to have airflow to achieve a respirable size cut (50% cutoff size of 4.0 μm). Airflows were calibrated before and after sample collection with a secondary airflow calibrator (TetraCal, Mesa Labs, Butler, NJ).

Before and after field sampling, all filters were conditioned at constant temperature and relative humidity for ≥24-hr. They were then weighed on a microbalance (MT5, Mettler-Toledo LLC, Columbus, OH). Respirable mass concentration was calculated as the mass gained during sampling divided by the volume of air sampled. CF was calculated as the gravimetric mass concentration from the filter sampler divided by the mean concentration measured by the photometer over the same time that the filter sampler was operated. After gravimetric analysis, filter samples from the pDR1500s were analyzed for metals by field portable X-Ray Fluorescence analyzer (FP-XRF, Niton XL3t Ultra, ThermoFisher Scientific, Waltham, MA) operated in thin film (“filter”) mode (detailed methods are provided in the Supplemental Information).

Data analysis

Linear regression was conducted to compare the calibration parameters of each sensor (intercept and slope), study the effect of time (weeks of deployment in the field) on each sensor calibration parameter, and characterize the relationship between sensor calibration parameters and the average weekly photometric-equivalent mass concentration as measured by the pDR1000. A box-and-whisker plot was prepared to display the mean, quartiles, and

minimum and maximum CFs calculated for pDR1500 and respirable filters. A paired t-test was conducted to compare means of the CFs grouped by locations. Regression analysis was performed in MATLAB R2017a (Natick, MA), and statistical tests were carried out in SAS (Version 9.4, SAS Institute Inc., Cary, NC) at a significance level of $\alpha = 0.05$.

Maps of PM concentration were prepared from monitor data. The database was accessed remotely and the raw data were uploaded and plotted using MATLAB. To compare the effects of area-specific CFs, a common field calibration slope and sensor-specific intercepts were used to convert sensor output from voltage to mass concentration. Two maps of respirable concentration were then prepared with: (1) a single, mean CF determined at the central location; and (2) using location-specific CFs determined throughout the facility. A third map was created to display the difference between the two maps applying different CFs.

Results and Discussion

Sensor calibration parameters

The overall linear regression for the 8-month deployment between each of the three co-located sensors and uncorrected (i.e., raw) pDR1000 concentration as well as the mean linear regression line (shown by a dashed line) with corresponding linear regression equations are shown in Figure 2. The overall field calibration slopes and intercepts for each sensor were statistically significantly different ($\alpha = 0.05$; Table S1. These calibration slopes and intercepts determined in the field were statistically significantly different compared to the laboratory slopes and intercepts ($\alpha = 0.05$; Table S1). The higher laboratory slope values were attributed to differences in the properties of the aerosol used in the laboratory (salt) compared to those of the aerosol in the field, such as size distribution and refractivity. It has been shown that optical sensor output signal is much lower for aerosols from welding fumes compared with salt particles.[21] These intercept results support the suggestion by Sousan et al.[22] to use a unique intercept for each sensor.

Weekly field calibration intercepts and slopes, along with uncorrected pDR1000 photometric-equivalent mass concentrations over the study period are shown in Figure 3 (upper, middle and bottom panels, respectively). There are gaps in the data because the pDR1000 lost power from November 19th until December 20th and from January 27th until March 22nd. As expected, diurnal variations in mass concentration are visible with the highest concentrations observed during the day shift and lowest on nights and weekends according to the photometric-equivalent mass concentrations from the pDR1000. Temporal variability was observed in the weekly calibration slopes for each sensor (shown by the circles, squares, and triangles for sensors 1, 2, and 3, respectively, in Figure 3). The weekly calibration slopes were relatively steady from August to September but less so from November through the end of the study. Sensor field calibration slope generally appears to decrease over time, but for weekly pDR1000 concentrations above the sensor limit of detection (0.026 mg/m^3), no statistically significant trend was observed for the calibration slope over time (mean change in slope = −2.2 $mV/(mg/m^3)$ per week; sensor-specific details provided in Table S2). During the Holiday season at the end of December 2017 and beginning of January 2018, all three sensors had substantially higher field calibration slopes

which were omitted because the average weekly pDR1000 photometric-equivalent mass concentrations were below 0.026 mg/m^3. Despite no clear temporal trend in the calibration slope, the variability does have consequences on PM measurements. Taking the median response (in millivolt) of each sensor for the 8-month deployment as an example (and using each sensor's overall field intercept), applying the maximum and minimum weekly calibration slopes for each sensor resulted in differences of photometric-equivalent mass concentration equal to 0.120, 0.180, and 0.100 mg/m^3, for sensors 1, 2, and 3, respectively.

The field calibration intercepts for each sensor increased with each passing week of the study period (mean increase = 1.5 mV per week), although this increase was only statistically significant for two of the three sensors (Table S1). Using each sensor's overall field slope and applying the maximum and minimum weekly calibration intercepts for each sensor resulted in differences of photometric-equivalent mass concentration equal to 0.180, 0.150, and 0.210 mg/m^3, for sensors 1, 2, and 3, respectively. In previous work, changes in sensor intercept were managed for all the sensors in the network by estimating a surrogate for weekly intercepts according to the response of each sensor in the absence of aerosol ('zero' concentration), approximated during low-concentration time periods.[25] Figure S1 displays the calibration intercept and zero of each of the three co-located sensors over time (panel a) and a regression comparison (panel b), demonstrating the sensor zero was comparable to the regression intercepts derived with a higher-quality photometer for the three co-located sensors (root mean square error, RMSE = 10 mV).

The general decrease in sensor slope and increase in intercept suggest that the sensor optics became dirty over the course of the deployment, although degradation of sensor components is also plausible. Aerosol passing through the sensor may land on the light emitting diode (light source), the photodiode (signal collector), or the light focusing lenses of both the light source and collector. The net effect of this deposition in the sensor appeared to cause a decrease in sensitivity (responsiveness to increasing aerosol concentration) and an increase in sensor baseline (response in the absence of aerosol) in this study. The process of sensor fouling and its consequence on sensor signal is the subject of forthcoming research.

The relationship between weekly field calibration slopes and intercepts and average weekly pDR1000 photometric-equivalent mass concentrations were also investigated (Figure 4). Weekly calibration slopes for photometric-equivalent mass concentrations greater than the sensor's limit of detection varied with average photometric-equivalent mass concentration (Figure 4; mean change in slope = −1,647 mV/(mg/m3) per mg/m^3; sensor-specific details provided in Table S2). Weekly field calibration intercepts for each sensor also varied with increasing average photometric-equivalent mass concentration but in a positive relationship (mean change in intercept = 543 mV per mg/m^3). All regression analyses suffered from poor fit (low R^2), suggesting the linear models used did not represent the relationship between changes in sensor calibration parameters and time or photometric-equivalent mass concentration as measured by the pDR1000 well. Consequently, caution is urged against overinterpreting these regression results and suggests general/qualitative evaluation.

Gravimetric correction factors

Gravimetric mass concentrations, photometric-equivalent mass concentrations, and CFs by sampling location are shown in Table 1. The locations were divided into four groups: (1) machining and welding; (2) cutting and shot blasting; (3) the central location; and (4) personal measurements made throughout the facility. Gravimetric mass concentrations were highest in March and lowest in December due to lower work activity. The means, quartiles, minimum, and maximum CFs for four location groups are summarized using box-and-whisker plots in Figure 5. CFs in the machining and welding area (4.6 ± 1.0) were not significantly different from those observed during personal sampling (5.1 ± 0.6). The central location mean CF of 3.7 ± 0.9 was significantly different than personal mean CF ($p = 0.03$). The central location mean CF was not significantly different than the machining and welding mean CF ($p = 0.16$), which is expected since it was located in a machining and welding area. The mean CF in the cutting and shot blasting area (2.9 ± 0.1) was substantially lower than all other groups. The difference between machining and welding CFs and cutting and shot blasting CFs was statistically significant ($p = 0.009$).

The variations in CFs at different locations were most likely due to different aerosol size distribution and composition present at these locations, which result in different aerosol optical properties. For example, the aerosol from the cutting and blasting area may be of larger size and similar composition to the metal sheets used to make parts and pieces compared to machining and welding areas where aerosol is composed of cutting oil mist and small-particle welding fume. The output from photometric sensors are different for the same mass concentration of different particle types.[21,26] Applying a single CF determined at a central location to all sensors across the facility,[25] does not take into account PM optical properties and size distribution variations at different locations. Li and Biswas[28] noted that using the same calibration parameters for different aerosol types could result in the error of over 400% in the mass concentration due to fivefold variation in the calibration factors.

Interestingly, CFs were strongly linearly related to respirable mass concentrations at the central location ($R^2 = 0.95$) and in personal measurements ($R^2 = 0.83$) (Figure 6). Correction factors from all other locations (i.e., machining & welding and cutting & blasting areas) did not follow a linear dependence with the concentration as strongly and were generally in-between the central location and personal CFs. This linear dependence may relate to the interaction of sources and general exhaust ventilation. When concentrations are low, the primary source of aerosol is from distant sources or from air handling units. In contrast, local sources will dominate when concentrations are high. These different sources likely have different optical properties and result in the dependency of CFs on concentration.

Maps of gravimetric-equivalent mass concentration produced using a single, mean CF (Figure 7a) are qualitatively similar to those produced using location-specific CFs (Figure 7b). The differences between them are shown in Figure 7c, and in some locations are over 0.2 mg/m^3. The fact that these maps appear similar is not surprising, given that the same mean CF (3.7) was used for the middle 1/3 of both maps and that the CFs determined at other locations were not that different (2.9 for cutting and blasting; 4.6 for machining and welding). Thus, although the CF varies with particle composition and size distribution, maps may be sufficiently accurate without being divided into regions with defined aerosol types

and separate calibration parameters applied to these regions, if the goal is to observe overall spatial patterns.

Gravimetric samples from different areas of the facility had similar metal compositions and proportions to one another: Fe ~35%; other ~59%; Mn 6%; Ni, Zn, and Cu < 1%. Details of the metal analysis are provided in the Supplemental Information (text and Figure S2).

Conclusions

In this study, the sources of variability of sensor calibration and CF variability were measured at a heavy vehicle manufacturing plant. The weekly calibration slopes and intercepts for each of three co-located sensors varied temporally from their overall slopes and intercepts for the total deployment period. In the present study, each of three co-located sensors in a network had specific and variable calibration slopes. In a previous work, applying the overall mean field calibration slope of these three sensors to all of the sensors in the network was a necessary accommodation to simplify calibration due to practical constraints at the study site, although it introduced error in photometric-equivalent mass concentrations. In this study, sensor calibration intercepts were identified to vary temporally and without correction will lead to measurement error. A limitation of this study is that only one location (central location) was used for co-locating pDR1000 and three low-cost sensors, and this study design prevented any observation as to whether the calibration parameters of sensors in various locations at the facility changed differently than those located at the central location. For example, the “dirtiest” locations in the facility may be within areas with different manufacturing processes. Variability in the CF across the facility was significant, ranging from 2.8 in the cutting and shot basting area to 6.3 in the machining and welding area. Thus, different CFs are recommended for different work processes in order to more accurately estimate gravimetric-equivalent mass concentrations with low-cost sensors.

Supplementary Material

Refer to Web version on PubMed Central for supplementary material.

Acknowledgments

Funding

This work was supported by the U.S. National Institute for Occupational Safety and Health under Grant R01 OH010533. C. Zuidema was supported by the Johns Hopkins University Education and Research Center for Occupational Safety and Health (ERC), which is funded by NIOSH under grant number T42 OH 008428, and the University of Washington’s Biostatistics, Epidemiology, and Bioinformatics Training in Environmental Heath (BEBTEH), grant number T32ES015459, from the National Institute for Environmental Health Science (NIEHS).

References

[1]. Akbarzadeh MA, Khaheshi I, Sharifi A, et al.: The association between exposure to air pollutants including PM10, PM2.5, ozone, carbon monoxide, sulfur dioxide, and nitrogen dioxide concentration and the relative risk of developing STEMI: A case-crossover design. Environ. Res 161:299–303 (2018). [PubMed: 29178978]

[2]. Liang HQ, Qiu H, and Tian LW: Short-term effects of fine particulate matter on acute myocardial infraction mortality and years of life lost: A time series study in Hong Kong. Sci. Total Environ 615:558–563 (2018). [PubMed: 28988091]

[3]. Otelea MR, Arghir OC, Zugravu C, Naghi E, Antoniu S, and Rascu A: Lung function and quality of life in workers with chemical and dust exposure. Rev. Chim 69(2):346–349 (2018).

[4]. MacLeod JS, Harris MA, Tjepkema M, Peters PA, and Demers PA: Cancer risks among welders and occasional welders in a national population-based cohort study: Canadian Census Health and Environmental Cohort. SH W 8(3):258–266 (2017).

[5]. OSHA: TABLE Z-1 Limits for Air Contaminants, 2012 Available at https://www.osha.gov/laws-regs/regulations/standardnumber/1910/1910.1000TABLEZ1 (accessed June 20, 2019).

[6]. ACGIH: Threshold Limit Values and Biological Exposure Indicies. 2019 American Conference of Governmental Industrial Hygienists Cincinnati, OH.

[7]. Wu CF, Delfino RJ, Floro JN, et al.: Evaluation and quality control of personal nephelometers in indoor, outdoor and personal environments. J. Exposure Anal. Environ. Epidemiol 15(1):99–110 (2005).

[8]. Koehler KA, and Peters TM: New methods for personal exposure monitoring for airborne particles. Curr. Environ. Health Rep 2(4):399–411 (2015). [PubMed: 26385477]

[9]. Gorner P, Bemer D, and Fabries JF: Photometer measurement of polydisperse aerosols. J. Aerosol Sci 26(8):1281–1302 (1995).

[10]. Molenar JV: Theoretical Analysis of PM2.5 Mass Measurements by Nephelometry. PM2000: Particulate Matter and Health. In Specialty Conference Charleston, SC: Air & Waste Management Association, 2000.

[11]. Wallace LA, Wheeler AJ, Kearney J, et al.: Validation of continuous particle monitors for personal, indoor, and outdoor exposures. J. Exposure Anal. Environ. Epidemiol 21(1):49–64 (2011).

[12]. Wang ZC, Calderon L, Patton AP, et al.: Comparison of real-time instruments and gravimetric method when measuring particulate matter in a residential building. J. Air Waste Manage. Assoc 66(11):1109–1120 (2016).

[13]. Sousan S, Koehler K, Hallett L, and Peters TM: Evaluation of consumer monitors to measure particulate matter. J. Aerosol Sci 107:123–133 (2017). [PubMed: 28871212]

[14]. Fischer SL, and Koshland CP: Field performance of a nephelometer in rural kitchens: effects of high humidity excursions and correlations to gravimetric analyses. J. Exposure Anal. Environ. Epidemiol 17(2):141 (2007).

[15]. Trent A: Laboratory Evaluation of New Real-time Smoke Particulate Monitors. Missoula, MT: U.S. Department of Agriculture, Forest Service, Missoula Technology and Development Center, 2003.

[16]. Malm WC, and Hand JL: Comparison between continuous and integrated mass measurements: Cooperative Institute for Research in the Atmosphere, Colorado State University, Fort Collins, CO, 2013.

[17]. Herbig B, Jorres RA, Schierl R, et al.: Psychological and cognitive effects of laser printer emissions: A controlled exposure study. Indoor Air 28(1):112–124 (2018). [PubMed: 28960517]

[18]. Peters TM, Heitbrink WA, Evans DE, Slavin TJ, and Maynard AD: The mapping of fine and ultrafine particle concentrations in an engine machining and assembly facility. Ann. Occup. Hyg 50(3):249–257 (2006). [PubMed: 16361396]

[19]. Evans DE, Heitbrink WA, Slavin TJ, and Peters TM: Ultrafine and respirable particles in an automotive grey iron foundry. Ann. Occup. Hyg 52(1):9–21 (2008). [PubMed: 18056626]

[20]. Liu S, and Hammond SK: Mapping particulate matter at the body weld department in an automobile assembly plant. J. Occup. Environ. Hyg 7(10):593–604 (2010). [PubMed: 20803369]

[21]. Sousan S, Koehler K, Thomas G, et al.: Intercomparison of low-cost sensors for measuring the mass concentration of occupational aerosols. Aerosol Sci. Technol 50(5):462–473 (2016). [PubMed: 28867868]

[22]. Sousan S, Gray A, Zuidema C, et al.: Sensor selection to improve estimates of particulate matter concentration from a low-cost network. Sensors 18(9):3008 (2018).

[23]. Jovašević-Stojanović M, Bartonova A, Topalović D, Lazović I, Pokrić B, and Ristovski Z: On the use of small and cheaper sensors and devices for indicative citizen-based monitoring of respirable particulate matter. Environ. Pollut 206(Supplement C):696–704 (2015). [PubMed: 26342459]

[24]. Thomas G, Sousan S, Tatum M, et al.: Low-cost, distributed environmental monitors for factory worker health. Sensors 18(5):1411 (2018).

[25]. Zuidema C, Sousan S, Stebounova LV, et al.: Mapping occupational hazards with a multi-sensor network in a heavy-vehicle manufacturing facility. Ann. Work Exposures Health 63(3):280–293 (2019).

[26]. Wang Y, Li J, Jing H, Zhang Q, Jiang J, and Biswas P: Laboratory evaluation and calibration of three low-cost particle sensors for particulate matter measurement. Aerosol Sci. Technol 49(11): 1063–1077 (2015).

[27]. Rea AW, Martin F, and Mitchell WJ: Evaluation of a Personal Nephelometer for Human Exposure Monitoring. Research Triable Park, NC, 2000.

[28]. Li JY, and Biswas P: Optical characterization studies of a low-cost particle sensor. Aerosol Air Qual. Res 17(7):1691–1704 (2017).

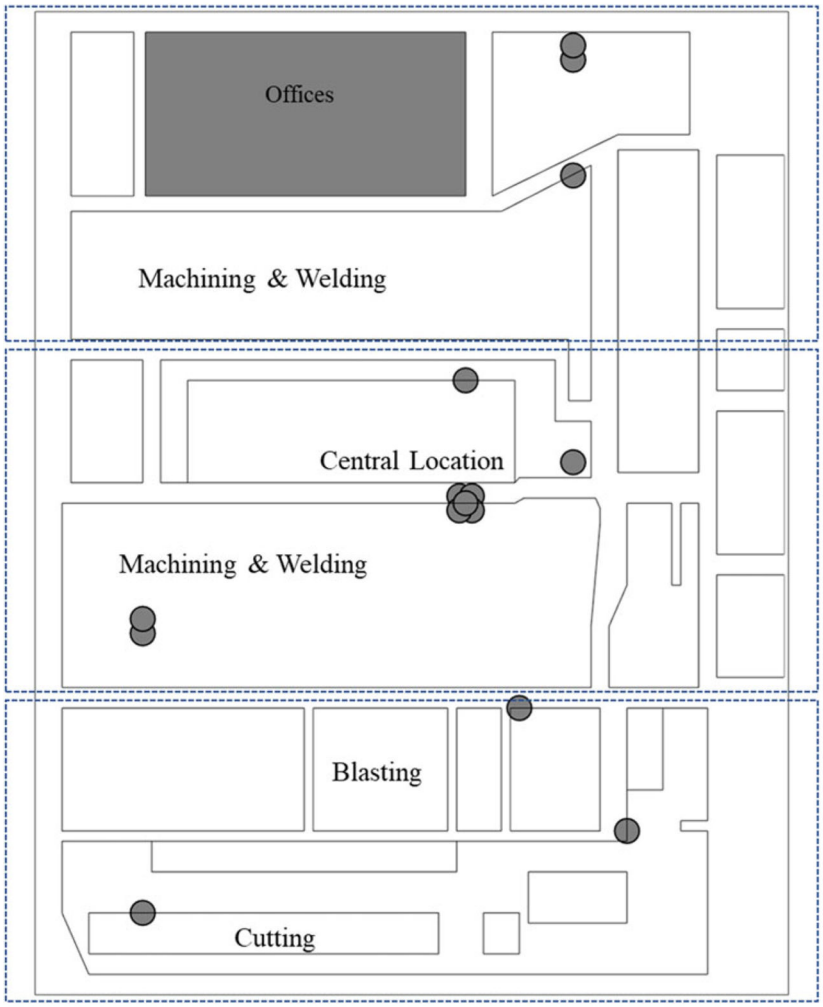

Figure 1.

Locations on the facility floor where filter samples were taken to measure gravimetric mass concentration and calculate gravimetric correction factors (CFs). At the central location, respirable cyclone filter samples were taken on 5 separate days (n=5). At all other locations, the internal filters of the pDR1500s configured for the respirable PM size fraction were used (n=10). Personal samples (n=8) were also collected, but are not shown on this figure because they were collected as study staff moved throughout the manufacturing floor. The dashed boxes denote areas of the manufacturing floor grouped together based on process and location.

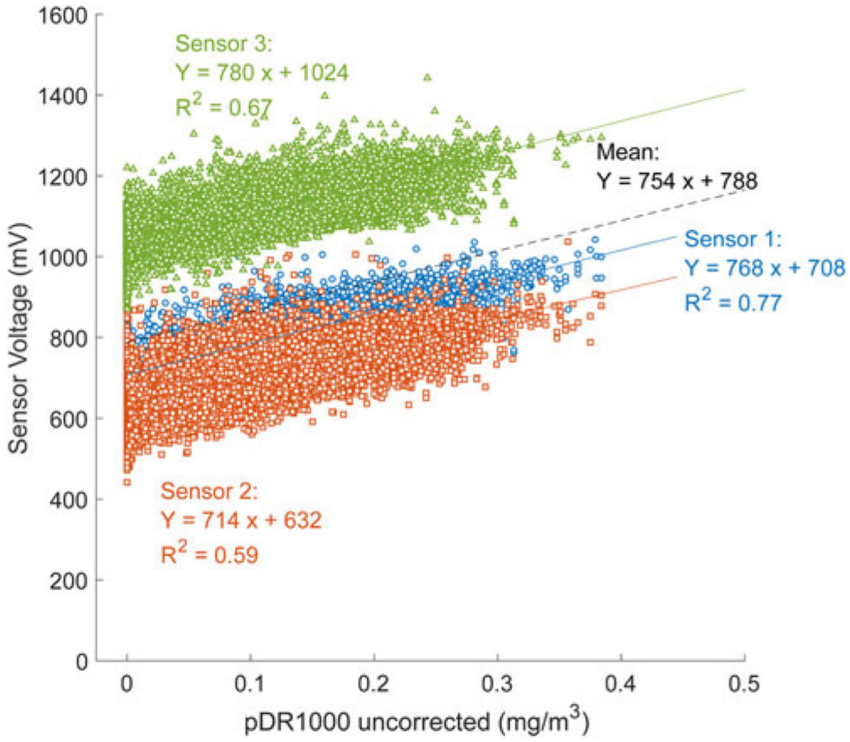

Figure 2.

Overall calibration used to convert sensor voltage to photometric-equivalent mass concentration at the central location for the 8-month deployment. Linear regressions for the three co-located low-cost sensors were plotted against 5-minute uncorrected (i.e., raw) pDR1000 photometric-equivalent mass concentrations. Circles, squares, and triangles show data points for sensors 1, 2, and 3, respectively. Solid lines show linear regressions of each individual sensor and the dashed line represents mean linear regression of the three co-located sensors.

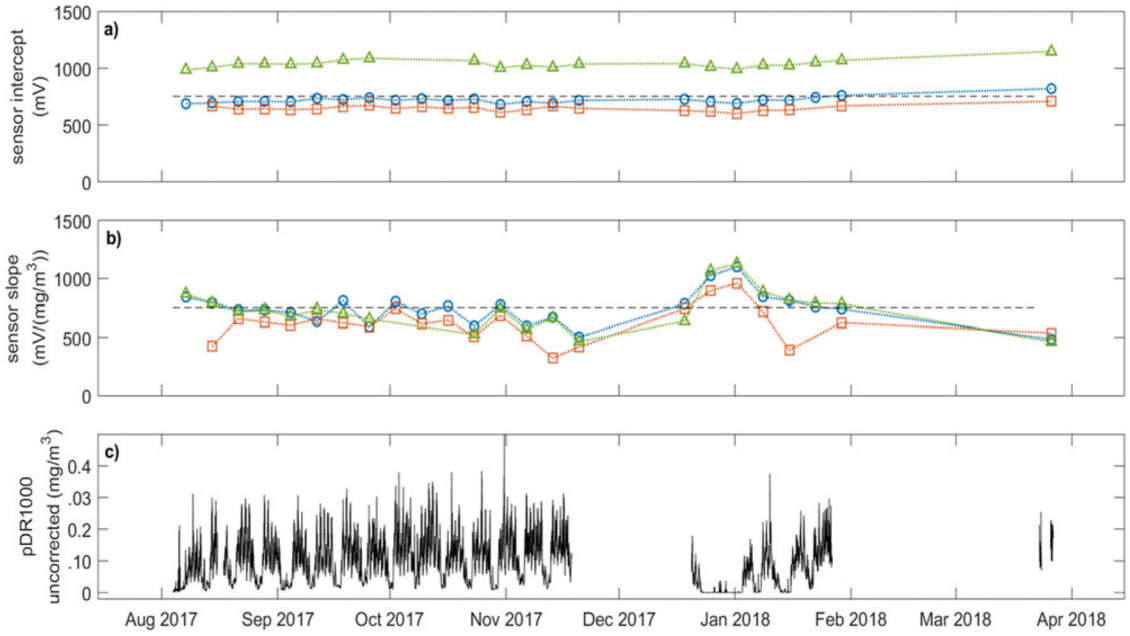

Figure 3.

Weekly sensor a) field intercepts and b) field slopes and c) uncorrected (i.e., raw) pDR1000 photometric-equivalent mass concentrations over the whole study period. Sensors 1, 2, and 3 are represented by the circle, square, and triangle, respectively. The horizontal dashed line represents the mean overall slope of 754 mV/(mg/m^3) and mean overall intercept of 788 mV for reference. All data were collected from the central location.

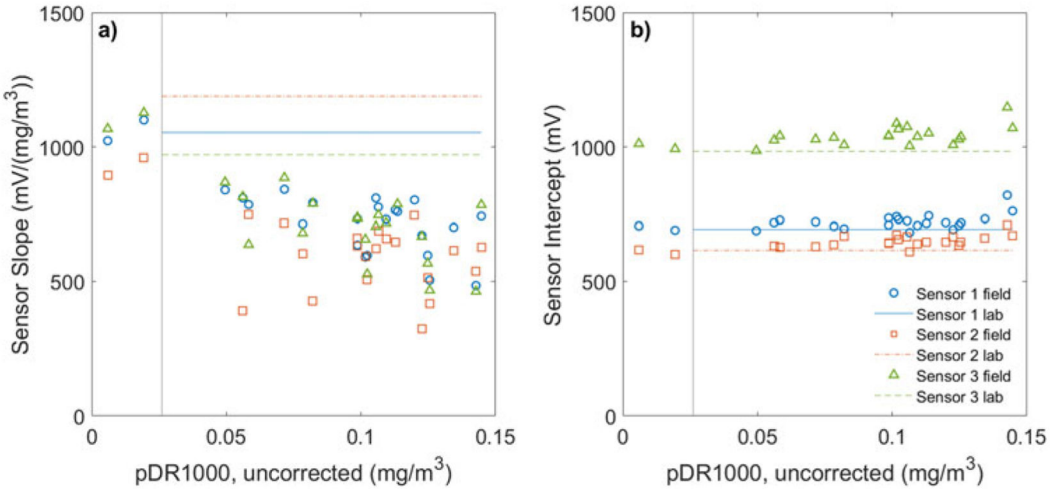

Figure 4.

Weekly calibration a) field slopes and b) field intercepts for each sensor versus weekly mean uncorrected (i.e., raw) pDR1000 photometric-equivalent mass concentration. Symbols are weekly field calibration parameters and horizontal lines are laboratory-derived calibration parameters. Vertical lines are drawn at the PM sensor limit of detection (0.026 mg/m^3), below which data were omitted from statistical analyses.

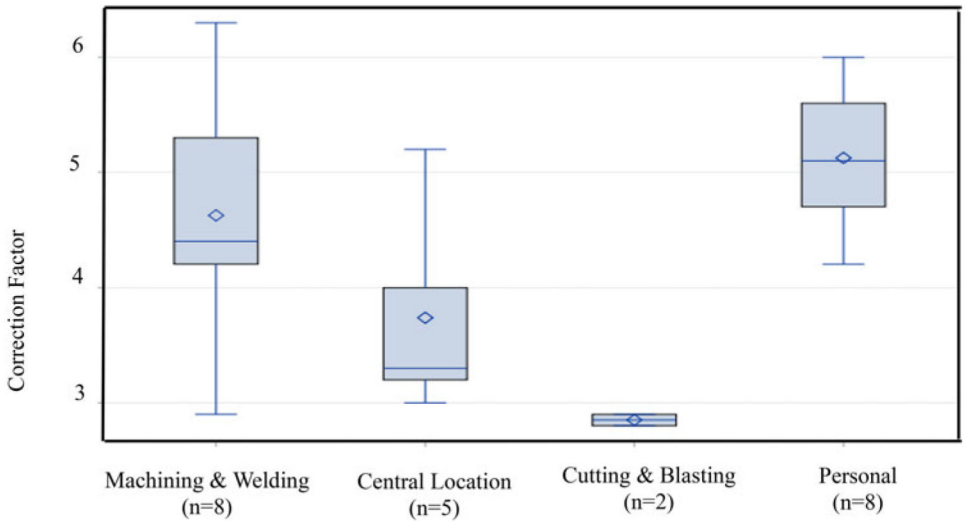

Figure 5.

Box-and-whisker plot showing the means, quartiles, minimums, and maximums of CFs stratified by location. Number in parentheses indicates sample size for each group.

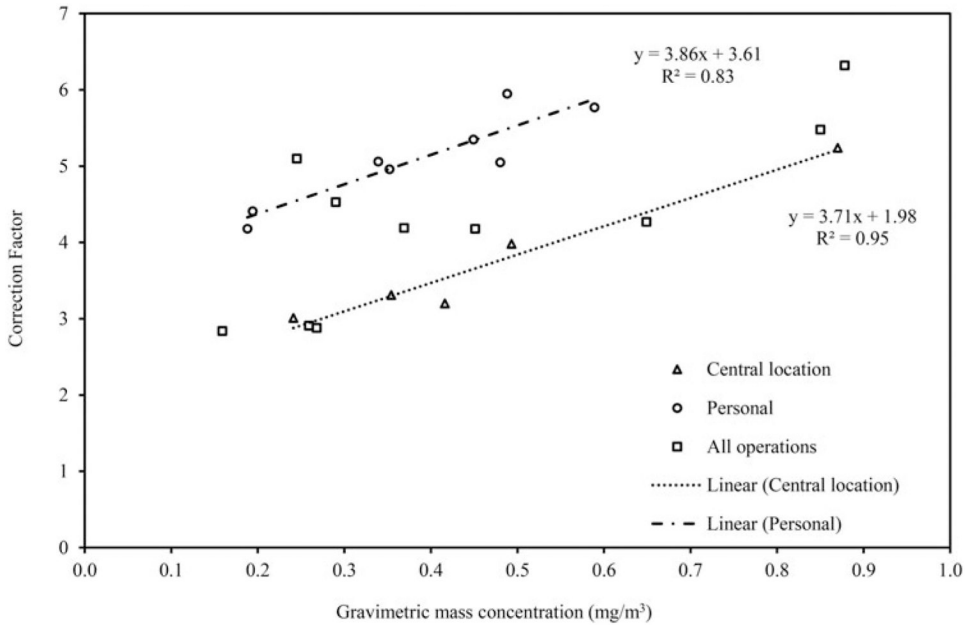

Figure 6.

Concentration dependence of the CFs and linear regressions for the central location and personal CFs. All operations refer to measurements taken in Machining & Welding and Cutting & Blasting areas.

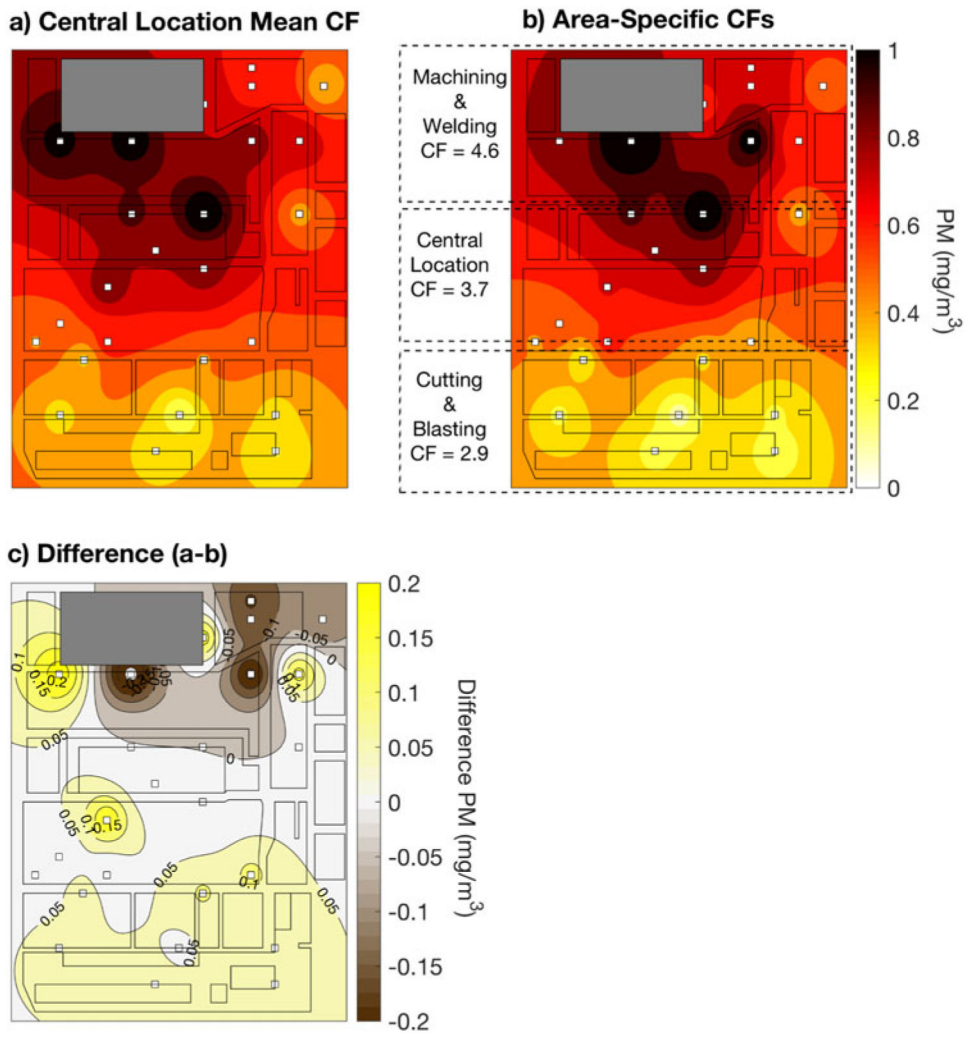

Figure 7.

Maps of gravimetric-equivalent mass concentration for the same time period (August 17, 2017, 8:00-8:55 am) using a common calibration slope and sensor-specific intercepts. In panel a, the mean CF from the central location (3.7) was applied. In panel b, location-specific CFs determined throughout the facility were applied as identified in the figure. Panel c displays the difference between panels a and b. Squares indicate locations of sensor network nodes.

Table 1.

Gravimetric correction factors (CFs) by location. Gravimetric mass concentrations were obtained with integrated filter samples. At the central location a respirable PM cyclone and filter collected the gravimetric sample and a pDR1000 collected the photometric-equivalent mass concentration measurements. At all other locations, a pDR1500 collected the photometric-equivalent mass concentration and the internal filter of the pDR1500, set up for the respirable PM size fraction, collected the gravimetric sample. Photometric-equivalent mass concentrations were averaged over the same time period when the gravimetric sample was collected. The specific locations of these samples are presented in Figure 1 (except personal samples).

Sample location	Month of field visit	Gravimetric mass concentration, mg/m^3	Photometric-equivalent mass concentration, mg/m^3	CF
Machining and Welding	August	0.451	0.108	4.2
	August	0.290	0.064	4.5
	December	0.369	0.088	4.2
	December	0.268	0.093	2.9
	December	0.245	0.048	5.1
	March	0.850	0.155	5.5
	March	0.649	0.152	4.3
	March	0.878	0.139	6.3
Cutting and Shot Blasting	December	0.159	0.056	2.8
	March	0.259	0.089	2.9
Personal	August	0.480	0.095	5.1
	August	0.449	0.084	5.4
	December	0.339	0.067	5.1
	December	0.352	0.071	5.0
	December	0.194	0.044	4.4
	December	0.188	0.045	4.2
	March	0.589	0.102	5.8
	March	0.488	0.082	6.0
Central Location	August	0.416	0.130	3.2
	December	0.354	0.107	3.3
	December	0.241	0.080	3.0
	March	0.493	0.124	4.0
	March	0.870	0.166	5.2